Solar Energy Materials & Solar Cells 114 (2013) 186–191

Contents lists available at SciVerse ScienceDirect

Solar Energy Materials & Solar Cells

journal homepage: www.elsevier.com/locate/solmat

Thermal aging characteristics of CrN_xO_y solar selective absorber coating for flat plate solar thermal collector applications

Liang Wu [a], Junhua Gao [a], Zhimin Liu [a], Lingyan Liang [a], Fei Xia [b], Hongtao Cao [a,*]

[a] Division of Functional Materials and Nano Devices, Ningbo Institute of Materials Technology & Engineering (NIMTE), Chinese Academy of Sciences (CAS), Ningbo 315201, People's Republic of China

[b] Division of Research and Development, Royal Tech. Solar, Changzhou 213163, People's Republic of China

ARTICLE INFO

Article history:
Received 29 September 2012
Received in revised form
25 February 2013
Accepted 7 March 2013

Keywords:
Solar selective absorber coating
CrN_xO_y
Thermal stability
Magnetron sputtering

ABSTRACT

A solar selective absorber coating of CrN_xO_y/SiO_2 was prepared on Cu (Si) substrate using DC reactive magnetron sputtering technique. The coating exhibits a high absorptivity (α) of 0.947 and a low emissivity (ε) of 0.05 at 80 °C. The spectral selectivity (α/ε) of the coating on Cu substrate is stable (0.930/0.073) even after heat-treatment at 278 °C in air for 300 h, but decreased (0.904/0.135) at 278 °C for 600 h. The determinants to govern the thermal stability were investigated by micro-Raman spectroscopy, X-ray photoelectron spectroscopy (XPS) and Auger electron spectroscopy (AES) measurements, which reveal that the element diffusion whether throughout all the stacked layers or near the interface region, the chemical interactions adjacent to the interface, and the interface width broadening are the Achilles' heel for the solar thermal coatings to sustain high thermal stability.

1. Introduction

The solar selective absorber coatings have attracted much attention for their applications in solar photo-thermal conversion [1–3]. Such coatings simultaneously possess high solar absorptivity (α) in the wavelength range of 0.3–2.5 μm and low thermal emissivity (ε) in the infrared region of 2.5–20 μm [4,5]. The ratio of α to ε, so-called solar selectivity, is used to evaluate the spectral properties of solar selective absorber coatings. For the purpose of achieving the spectral selectivity, various concepts and materials have been explored so far [1–6].

At present, absorber coatings with acceptable thermal stability are commercially available in the market. However, there is a continuous need to increase the thermal stability, in order to keep the solar–thermal converting efficiency constant in the whole life time. Generally, transition metal nitride/oxynitride has good performance as a diffusion barrier due to its high-temperature oxidation resistance. Accordingly, in recent years, transition metal or metal alloy nitride/oxynitride has been intensively investigated for solar thermal applications [4]. Chrome, like other transition metal elements, has been studied and developed in such research field. Fan and Spura reported that the sputtered Cr–Cr_2O_3 cermets deposited on Cu substrates were stable up to 200 °C with a solar selectivity of 0.90/0.12, whereas the cermets grown on nickel substrates showed good thermal stability up to 300 °C [7]. Teixeira et al. revealed that the graded Cr–Cr_2O_3 cermets exhibited a high absorptivity of 0.95 and a low emissivity of 0.05 [8]. Barshilia et al. investigated the evolution of structural and optical properties of $Cr_xO_y/Cr/Cr_2O_3$ solar selective coatings by pulsed sputtering technique, and found that the coatings were stable in air up to 250 °C for 250 h with a solar selectivity of 0.898/0.11 [9]. The optical and electronic properties of CrN_xO_y films, deposited by reactive DC magnetron sputtering in the $Ar/N_2/O_2(N_2O)$ atmospheres, were also studied by Mientus et al. [10]. Barshilia et al. reported the spectrally selective CrMoN/CrON tandem absorber for mid-temperature solar thermal applications, in which the optical properties of CrON had been studied [11]. Nevertheless, for the chromium-based oxynitride used as solar selective coatings, detailed information on the behaviors of element diffusion, chemical reaction or interaction, and the interface width fluctuation as a function of thermal treatment is still lacking.

In this work, DC reactive sputtering is used to deposit the CrN_xO_y/SiO_2 multilayer absorber coatings on Cu or Si substrates. The structural, chemical, and optical evolution of these coatings with thermal treatment was comprehensively investigated. According to the accelerated aging tests, the thermal aging characteristics of these coatings were analyzed and presented, which is indispensable to uncover the black box of element diffusion, chemical reaction/interaction, and interface width fluctuation of the studied coatings.

2. Experiment details

The CrN_xO_y coatings were prepared on Cu substrate (Si substrate as a reference) using a DC reactive magnetron sputtering

* Corresponding author. Tel.: +86 57486685161; fax: +86 57486685163.
E-mail address: h_cao@nimte.ac.cn (H. Cao).

0927-0248/$ - see front matter Crown Copyright © 2013 Published by Elsevier B.V. All rights reserved.
http://dx.doi.org/10.1016/j.solmat.2013.03.005

system (ULVAC JSP-8000) with a 2 inch Cr metallic target (99.95%). Before putting into the vacuum chamber, the substrates were chemically cleaned. After evacuating to a base pressure of 5.0×10^{-5} Pa, Cr–N/Cr–O/SiO_2 layers were deposited successively on Cu (Si) substrates. The microstructure and composition of the coatings were tuned by adjusting the gas flow rate and the target power, in the hope of reinforcing the solar spectrum selectivity. The optimized parameters to make the multilayer coatings are listed in Table 1.

To estimate the acceptable service life of an absorber coating, the International Energy Agency-Solar Heating and Cooling program (IEA-SHC), Task 27 [12–16], has defined an advanced performance criterion (PC) function for flat plate collector testing. The so-called performance criterion (PC) should be a useful property to describe the influence of the changes in the solar absorptivity $\Delta\alpha_s$ and the thermal emissivity $\Delta\varepsilon$, less important by the factor of 0.5, on the solar fraction:

PC=$\Delta\alpha_s$–0.5$\Delta\varepsilon$, where $\Delta\alpha_s=\alpha_s$ (unaged)–α_s (after testing) and $\Delta\varepsilon=\varepsilon$ (unaged)–ε (after testing) [12].

The maximum stagnation temperature was estimated to be 204 °C in line with Table 1 of Ref. [12]. The reason why 204 °C, as the expected stagnation temperature, is selected is based on the values of α=0.947 and ε=0.050 [12]. For this particular stagnation temperature, Table 2 of Ref. [12] yields a testing temperature of 278 °C, which was chosen in this study. To evaluate the thermal stability, the samples were annealed in air in a resistive tubular furnace at 278 °C for 18 h, 36 h, 75 h, 150 h, 300 h, and 600 h. The dependence of optical properties, microstructure, and chemical composition of the coatings on the thermal treatment was investigated. The absorptivity and emissivity were measured using a UV–vis–IR spectrophotometer (Perkin-Elmer Lambda 950) and an emissometer at 80 °C, respectively, and the detailed measurement procedures have been reported elsewhere [4,9]. Raman spectra were recorded using a micro-Raman spectrometer (Renishaw inVia Reflex, and a Nd:YAG laser with a wavelength of 532 nm was utilized) with a CCD detector at room temperature. The chemical bonding state study and the elemental depth profiling of the multilayer films were conducted by X-ray photoelectron spectroscopy (XPS, equipped with a standard monochromatic Al-Kα source ($h\nu$) 1486.6 eV, Kratos Analytical Ltd., UK) and Auger electron spectroscopy (AES), respectively. Primary electron beam energy of 10 keV was employed for the XPS and the AES measurements, and an Ar^+ energy of 4 keV with 100 μA ion current was utilized for the layer-by-layer etching. The XPS binding energy data were calibrated with respect to the C1s signal of ambient hydrocarbons (C–H and C–C) centered at 284.8 eV. The Lorentzian–Gaussian function after subtraction of a Shirley-type background was applied to fit the narrow scanning spectra of various elements, in which the chi-square value was minimized. Auger electron spectra were recorded in the integral ($N(E)/E$) mode. The integral Auger data were converted into the differential ($dN(E)/dE$) mode by using the commercially available Casa XPS software.

Table 1
The optimized processing parameters for the fabrication of CrN_xO_y/SiO_2 coatings.

Layer	Gas flow rate (sccm)			Power density (W/cm^2)	Substrate RF bias (W)	Thickness (nm)
	Ar	O_2	N_2			
SiO_2	10	0	0	5	0	100
Cr–O_M	4	1	0	4	100	30
Cr–O_D	4	0.8	0	4	100	30
Cr–N	4	0	3	4	100	45

The two Cr–O layers were deposited under different O_2 gas flowing rates. The subscripts *M* and *D* stand for the O_2 gas flowing rates at 1.0 sccm and 0.8 sccm, respectively.

Table 2
The effect of annealing at 278 °C for different times in air on the absorptivity, emissivity, and PC values of the Cu/CrN_xO_y/SiO_2 coatings deposited on copper substrates. The PC value describes the influence in the change of solar absorption ($\Delta\alpha_s$) and emissivity ($\Delta\varepsilon$) on the solar fraction: PC=$\Delta\alpha_s$–0.5$\Delta\varepsilon\leq$0.05 [12].

Time (h)	α	ε	$\Delta\alpha_s$	$\Delta\varepsilon$	PC
0	0.947	0.052	0	0	0
18	0.939	0.058	0.008	−0.006	0.011
36	0.945	0.053	0.002	−0.001	0.0025
75	0.937	0.065	0.010	−0.013	0.0165
150	0.935	0.069	0.012	−0.017	0.0205
300	0.930	0.073	0.017	−0.021	0.0275
600	0.904	0.135	0.043	−0.083	0.0845

3. Results and discussion

The schematic diagram of CrN_xO_y/SiO_2 multilayer structure is shown in Fig. 1. In this design, the first absorber layer (labeled with Cr–O_M) has a higher metallic content than the second one (labeled with Cr–O_D), so as to obtain distinct refractive indices to improve the optical properties. Although binary transition metal nitrides (such as CrN) do not exhibit high solar absorptivity [11], the layer of Cr–N can be used as the diffusion barrier [17]. The absorptivity could be further enhanced by depositing an anti-reflection coating on top of the absorbing layer.

Thermal stability of the solar absorber is very crucial because the absorber would definitely degrade with time at the operating temperatures, which shrinks the life time and eventually leads to failure.

Comparison of α and ε values of both the as-deposited and the annealed samples is given in Table 2. The as-deposited samples exhibit a high absorptivity of 0.947 and a low emissivity of 0.050 at 80 °C. The coatings were thermally stable in air at 278 °C for 300 h. For example, no significant changes were observed in the optical properties ($\Delta\alpha$=0.017/$\Delta\varepsilon$=−0.021). After 600 h, however, the emissivity increases significantly and the performance criterion (PC) value exceeds 0.05 [12]. These results indicate that the CrN_xO_y/SiO_2 coating is thermally stable in air within 300 h, but got degraded after 600 h.

To understand the thermal aging mechanisms, the microstructural properties of these CrN_xO_y/SiO_2 coatings with different annealing treatments were studied using micro-Raman spectroscopy, as demonstrated in Fig. 2. For the as-deposited samples, the broadening Raman bands centered at 660 cm^{-1} should correspond to the chromium-related complex oxides rather than Cr_2O_3. The Raman spectra of the heat-treated ones (278 °C for 18 h in air), however, display the excursion of main peak centered at 670 cm^{-1}

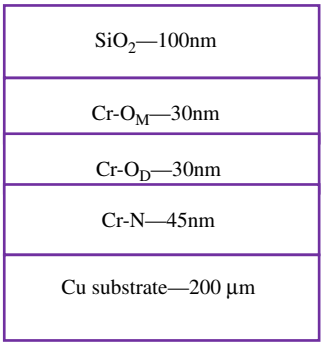

Fig. 1. Schematic diagram of the Cu/CrN_xO_y/SiO_2 absorber coating.

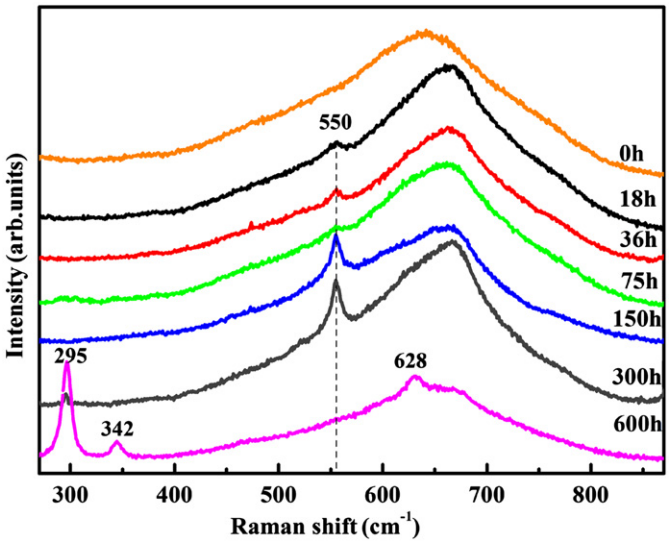

Fig. 2. The Raman spectra of the as-deposited Cu/CrN_xO_y/SiO_2 coating and coatings annealed at 278 °C for different times.

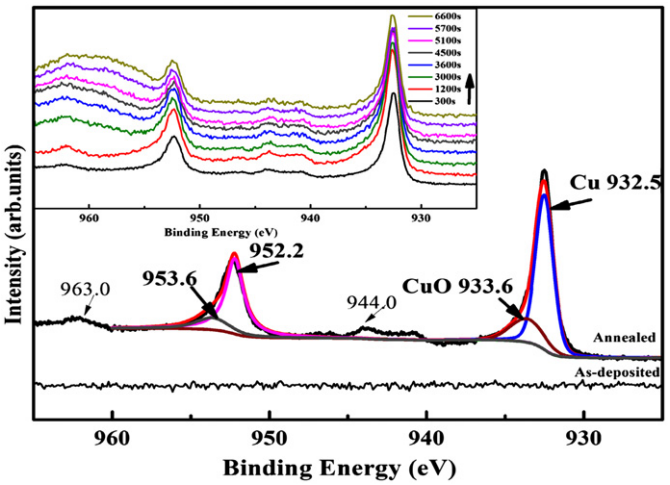

Fig. 3. The Cu 2p core level spectra of the Cu/CrN_xO_y/SiO_2 coatings before and after annealing. The Cu XPS signals of annealed samples could be detected in the uppermost SiO_2 layer after 300 s etching, whereas no Cu signals of the as-deposited samples could be found in the SiO_2 layer after 300 s etchings. The Cu XPS spectra with different etching times (i.e., different etch depths) were illustrated in the inset for the annealed samples.

and the presence of *A*1*g* (550 cm^{-1}) [9,18] bands of Cr_2O_3. Moreover, the intensity of the *A*1*g* peak increases gradually with the heat treating time, which means that the proportion of Cr_2O_3 is increasing. The shift of main peak to higher wavenumbers (from 660 to 670 cm^{-1}) is probably due to the valence state change of Cr. When the sample was annealed at 278 °C for 300 h, there is a very small CuO peak located at 295 cm^{-1} [19], which could be attributed to the inclusion of CuO into the coating after annealing. However, relative to the as-deposited specimen, three peaks of CuO centered at 295, 342 and 628 cm^{-1} [19] could be detected clearly after heat treatment for 600 h, and thus the main peak positions are obviously shifted. The emergence of CuO peaks could be ascribed to the Cu diffusion from the substrate into the absorber layers. In addition, the intermixing of Cu with CrN_xO_y, and in particular the formation of CuO, would lead to an increase of the emissivity [9].

To obtain the actual chemical composition of the samples, depth profiling was carried out by XPS combined with 4 keV Ar^+ sputtering. As expected, no signals related to Cu or CuO could be found in the as-deposited specimens, while the information about Cu and CuO was identified for the 600-h-annealed samples, even in the uppermost SiO_2 layer after 300 s etching, as demonstrated in Fig. 3. Two peaks located at (932.5 eV) and (952.2 eV) were stretched out, which correspond to Cu $2p_{3/2}$ and Cu $2p_{1/2}$ of metallic copper, respectively. Meanwhile the peaks centered at (933.6 eV) and (953.6 eV) could be assigned to Cu $2p_{3/2}$ and Cu $2p_{1/2}$ states of CuO, respectively. The doublet separation of 20.0 eV between Cu $2p_{3/2}$ (933.6 eV) and Cu $2p_{1/2}$ (953.6 eV) also confirms that the bonding state of copper is in the form of CuO [9,20]. Furthermore, two peaks located at 944.0 and 963.0 eV are also the characteristics of CuO [9]. It must be mentioned that the same information with depth profiling resolution was illustrated in the inset of Fig. 3, which gives evidence that the copper diffusion and the concomitant formation of CuO detected by the XPS technique, in good agreement with the Raman spectroscopy analysis, are the essential mechanisms to account for the coating degradation [9,21].

High temperature accelerated aging and stability testing may induce microstructure degradation such as interface diffusion, reaction between different layers to yield phase transformation and oxidation, and so on. In order to obtain accurate information about the interface interaction between alien layers, the Si/CrN_xO_y/SiO_2 coating, acting as a reference, was fabricated as usual and

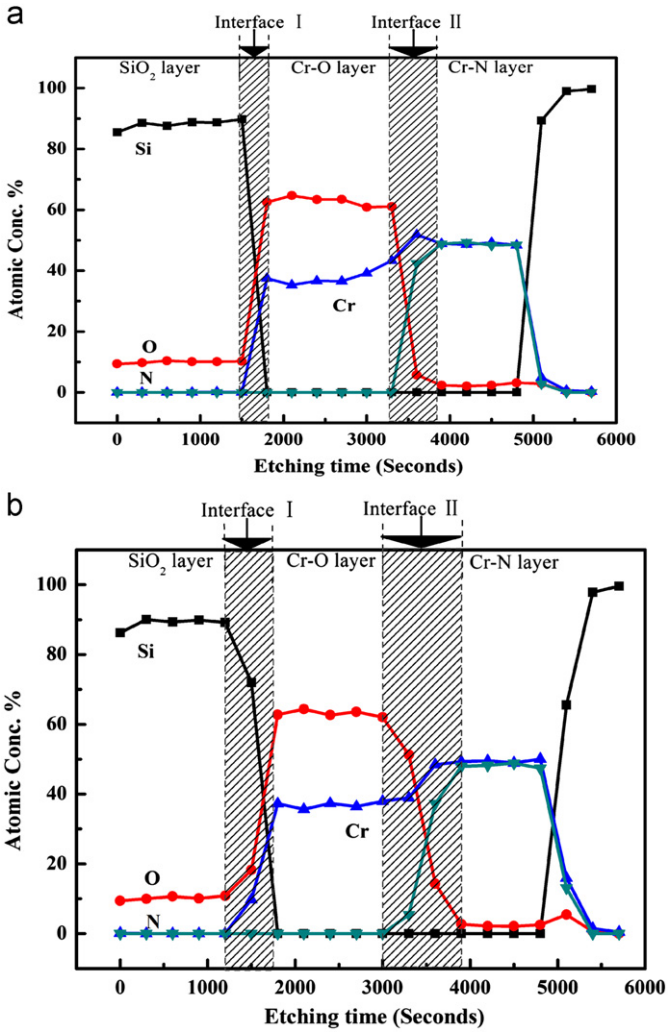

Fig. 4. AES analysis results of the Si/CrN_xO_y/SiO_2 coating: (a) as-deposited and (b) 278 °C treated for 300 h.

investigated with the aid of the Auger electron spectroscopy (AES) technique, in the hope of eliminating the influence of Cu substrates.

In-depth composition study of the coatings is illustrated in Fig. 4. On one hand, as shown in Fig. 4a, the SiO_2, Cr–O, and Cr–N layers can be identified unambiguously and the interfaces among them are sharp and clear. The atomic concentration close to the interface could rise or drop dramatically, indicating that no evident interfacial diffusion occurred. On the other hand, the profiles (shown in Fig. 4a) of the as-deposited coatings displayed homogeneous concentration throughout the entire coating. For comparison, the atomic concentration depth profiles for the 300 h heat-treated sample are also demonstrated in Fig. 4b. The SiO_2, Cr–O, and Cr–N layers can also be found correspondingly. However, the variation of the atomic concentration in the interface region I is changing more gently than the counterpart as shown in Fig. 4a, which manifests the annealing promotes the interfacial diffusion and broadens the interface width. A similar phenomenon is also observed in the interface region II between Cr–O layer and Cr–N layer. As a result, the above results once again confirm the existence of the interfacial diffusion in the studied coatings, which eventually brings about performance degradation.

It is believed that the chromium-related Auger energy varies more or less with the local chemical environment due to the change in the interior electron shells. Accordingly, the ability of the AES to reveal some detailed chemical information from local area allows investigating the reactions in the interface region. In many cases the chemical state of an element can also be inferred from the AES spectra in terms of the intensity, energy and lineshape of the specific peaks.

In this study, Auger spectra were obtained using the integral ($N(E)/E$) mode, and the integral Auger data were converted into the differential ($dN(E)/dE$) mode by the open-access software. Three specific peaks arising from the so-called $L_3M_{23}M_{23}$ (=LMM), $L_3M_{23}M_{45}$ (=LMV), and $L_3M_{45}M_{45}$ (=LVV) transitions that are summarized as the LMM group transition, appear in the high energy range of the chromium Auger spectra [22]. Fig. 5 displays the differential Auger electron spectra of Cr LMM group and oxygen KLL peaks for the CrN_xO_y/SiO_2 multilayers before and after 300 h-annealing, in which the information from the SiO_2, Cr–O,

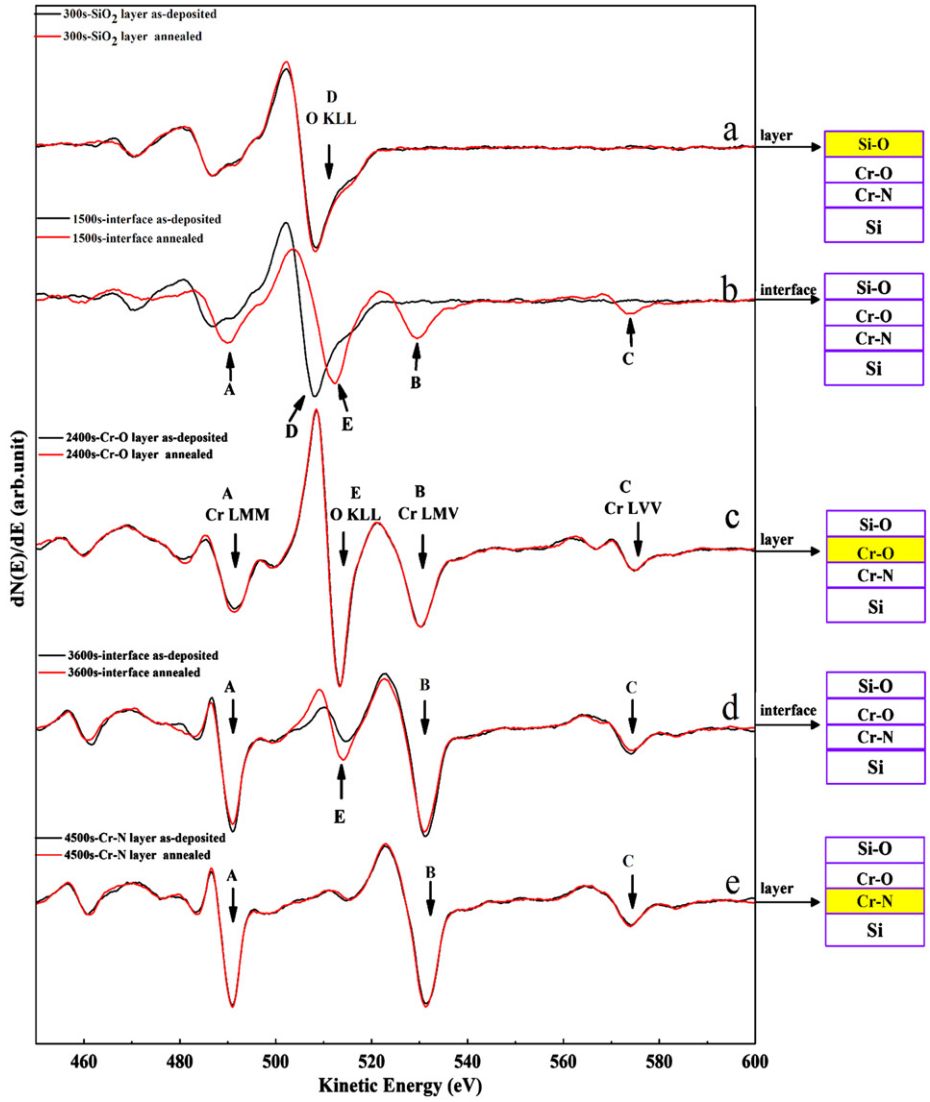

Fig. 5. Cr LMM group and O KLL Auger peaks for the as-deposited and annealed $Si/CrN_xO_y/SiO_2$ coatings. The specimens with an etching time of 300 s (a), 1500 s (b), 2400 s (c), 3600 s (d), and 4500 s (e). The symbols A, B and C stand for the Cr LMM, Cr LMV and Cr LVV Auger peaks respectively, D represents the O KLL Auger peak in the SiO_2 layer and E represents the O KLL Auger peak in the CrN_xO_y layer. (For interpretation of the references to color in this figure legend, the reader is referred to the web version of this article.)

and Cr–N layers corresponds to Fig. 5a, c, and e, respectively. Concerning Fig. 5a, c, and e, one can observe that the differential curves are coincident with each other before and after annealing, suggesting that there are no obvious changes in those layers. In particular, the O KLL Auger peak at 508.2 eV corresponds to the oxygen in silicon oxide (SiO_2 layer after 300 s etching, Fig. 5a). The kinetic energy of the Cr LMV Auger main peak in the Cr–O layer (Fig. 5c, with 3600 s etching time) is about 530.0 eV, whereas in the Cr–N layer (Fig. 5e, with 4500 s etching time) it is 531.5 eV. The O KLL Auger peak in the Cr–O layer is centered at 513.2 eV, revealing that the oxygen stems from the chromium oxides. It should be pointed out that no oxygen signal is detected within the Cr–N layer.

Fig. 5b and d highlight the AES signals coming from the interfaces between the adjacent layers. It is obvious that the differential curves differ from each other before and after annealing. The change in the shape of chromium-related Auger peaks involved in valence electron transitions can be distinctly noticed after annealing, as shown in Fig. 5b (interface region I with 1500 s etching time). After annealing, three specific Auger peaks related to chromium can be identified in the interface region I, implying that the diffusion of Cr element occurred. And most importantly, the intensity of the peaks present in Fig. 5b is relatively lower than the normal one which is shown in Fig. 5c. If strong chemical bonding among different elements occurs, the core electron levels may change a few electron volts. For example, the O KLL Auger peak at 512.2 eV (the red line in Fig. 5b) falls in between silicon oxide (508.2 eV) and chromium oxide (513.2 eV), indicating that the oxygen is in a more complicated chemical environment. To be specific, the interfacial interaction at the chromium oxide/silicon oxide interface (interface region I) occurs definitely. In the interface region II (Fig. 5d, 3600 s etching time), the intensity of the O KLL peaks after annealing is higher than that of the as-deposited. The reason is probably due to the boosted oxygen concentration after annealing or the annealing-induced interfacial interaction in the interface region II. The results suggest that the interfacial diffusion and interaction could be the stimuli to govern the performance degradation.

The annealing treatment of the CrN_xO_y/SiO_2 coatings in air may induce several microstructural modifications such as diffusion and oxidation of the Cu, interfacial reaction between different layers to generate new phases, interfacial diffusion, and so on, which results in severe changes in the optical properties. In this study, the degradation mechanisms of the CrN_xO_y/SiO_2 coatings annealed at 278 °C for 600 h are attributed to the factors as follows. (i) The diffusion of metallic Cu from the substrate into the rest layers is present definitely. In addition, the formation of CuO phase also takes place. (ii) The interfacial diffusion within a confined region and interactions close to the interface region are also expected to lead to performance degradation, since both the change of element atomic concentration and interface width broadening are experimentally observed.

4. Conclusions

A four-layer stacked CrN_xO_y/SiO_2 solar selective absorber coating was fabricated on Cu (Si) substrate by DC reactive magnetron sputtering technique, which exhibited a high absorptivity (α) of 0.947 and a low emissivity(ε) of 0.050 at 80 °C. The spectral selectivity (α/ε) of the coating fabricated on Cu substrate was maintained at 0.930/0.073 even after heat-treatment at the stagnation temperature of 278 °C in air for 300 h, but got degraded severely (0.904/0.135) after 600 h treatment. In this work we performed accelerated life testing to find out the determinants to govern the thermal stability of the coatings. On the basis of the diverse characterization techniques, on one hand, the element diffusion of Cu from the substrate throughout all the stacked layers (the diffusion length is long in distance), along with the concomitant generation of CuO phase, becomes one of the essential mechanisms to account for the coating degradation; on the other, the element diffusion close to the interface region (with finite diffusion length in nature), the chemical interactions adjacent to the interface, and the interface width broadening are expected to be other degradation models.

Acknowledgments

This work is supported by the Applied Research Funds for Public Welfare Project of Zhejiang Province (2011C21030), the Chinese National Program on Key Basic Research Project (2012CB933003), the National Natural Science Foundation of China (Grant no. 11104289), the Science and Technology Innovative Research Team of Ningbo Municipality (2009B21005), and the Key Program for Science and Technology Innovative Team of Zhejiang Province (2010R50020).

References

[1] N. Selvakumar, H.C. Barshilia, Review of physical vapor deposited (PVD) spectrally selective coatings for mid- and high-temperature solar thermal applications, Solar Energy Materials and Solar Cells 98 (2012) 1–23.
[2] C.E. Kennedy, Review of Mid and High Temperature Solar Selective Absorber Materials, Technical Report, NREL/TP-520-31267, National Renewable Energy Laboratory of USA, July 2002.
[3] M.A. Alghoul, M.Y. Sulaiman, B.Z. Azmi, M.A. Wahab, Review of materials for solar thermal collectors, Anti-Corrosion Methods and Materials 52 (2005) 199–206.
[4] Y. Liu, C. Wang, Y. Xue, The spectral properties and thermal stability of NbTiON solar selective absorbing coating, Solar Energy Materials and Solar Cells 96 (2012) 131–136.
[5] H. Barshilia, N. Selvakumar, K. Rajam, D. Sridhararao, K. Muraleedharan, Deposition and characterization of TiAlN/TiAlON/Si_3N_4 tandem absorbers prepared using reactive direct current magnetron sputtering, Thin Solid Films 516 (2008) 6071–6078.
[6] J.H. Schon, G. Binder, E. Bucher, Performance and stability of some new high temperature selective absorber systems based on metal/dielectric multilayers, Solar Energy Materials and Solar Cells 33 (1994) 403–416.
[7] J.C.C. Fan, S.A. Spura, Selective black absorbers using rf-sputtered Cr_2O_3/Cr cermet films, Applied Physics Letters 30 (1977) 511–513.
[8] E.S.V Teixeira, M.F. Costa, C. Nunes, L. Rosa, M.J. Carvalho, M. Collares-Pereira, E. Roman, J. Gago, Chromium-based thin sputtered composite coatings for solar thermal collectors, Vacuum 64 (2002) 299–305.
[9] H.C. Barshilia, N. Selvakumar, K.S. Rajam, A. Biswas, Structure and optical properties of pulsed sputter deposited Cr_xO_y/Cr/Cr_2O_3 solar selective coatings, Journal of Applied Physics 103 (2008) 023507-1–023507-11.
[10] R. Mientus, R. Grötschel, K. Ellmer, Optical and electronic properties of CrO_xN_y films, deposited by reactive DC magnetron sputtering in Ar/N_2/O_2(N_2O) atmospheres, Surface and Coatings Technology 200 (2005) 341–345.
[11] N. Selvakumar, S. Santhoshkumar, S. Basu, A. Biswas, Harish C. Barshilia, Spectrally selective CrMoN/CrON tandem absorber for mid-temperature solar thermal applications, Solar Energy Materials and Solar Cells 109 (2013) 97–103.
[12] M.K. Öhl, M. Heck, S. Brunold, U. Frei, B. Carlsson, K.M. Öller, Advanced procedure for the assessment of the lifetime of solar absorber coatings, Solar Energy Materials and Solar Cells 84 (2004) 275–289.
[13] S. Brunold, U. Frei, B. Carlsson, K. MÖller, M. KÖhl, Accelerated life testing of solar absorber coatings: testing procedure and results, Solar Energy 68 (2000) 313–323.
[14] R. Gampp, P. Oelhafen, P. Gantenbein, S. Brunold, U. Frei, Accelerated aging tests of chromium containing amorphous hydrogenated carbon coatings for solar collectors, Solar Energy Materials and Solar Cells 54 (1998) 369–377.
[15] B. Carlsson, K.M. Öller, M.K. Öhl, U. Frei, S. Brunold, Qualification test procedure for solar absorber surface durability, Solar Energy Materials and Solar Cells 61 (2000) 255–275.
[16] S. Brunold, U. Frei, B. Carlsson, K.M. Öller, M.K. Öhl, Round robin on accelerated life testing of solar absorber surface durability, Solar Energy Materials and Solar Cells 61 (2000) 239–253.
[17] Jui-Chang Chuang, Shuo-LunTu, Mao-Chieh Chen, Sputtered Cr and reactively sputtered CrN_x serving as barrier layers against copper diffusion, Journal of the Electrochemical Society 145 (1998) 4290–4296.

[18] S.H. Shim, T.S. Duffy, R. Jeanloz, C.S. Yoo, V. Iota, Raman spectroscopy and x-ray diffraction of phase transitions in Cr_2O_3 to 61 GPa, Physical Review B 69 (2004) 144107-1–144107-12.
[19] J.F. Xu, W. Ji, Z.X. Shen, W.S. Li, S.H. Tang, X.R. Ye, D.Z. Jia, X.Q. Xin, Raman spectra of CuO nanocrystals, Journal of Raman Spectroscopy 30 (1999) 413–415.
[20] J.Y. Park, Y.S. Jung, J. Cho, W.K. Choi, Chemical reaction of sputtered Cu film with PI modified by low energy reactive atomic beam, Appled Surface Science 252 (2006) 5877–5891.
[21] S.V. Krishnaswamy, L.L. Tongson, N. Said, R. Messier, Enhanced inter-diffusion of Cu into rf-sputtered chromium-oxide films, Journal of Vacuum Science and Technology 18 (1981) 401–404.
[22] Hua Lu, D.H. Shen, C.L. Bao, Y.X. Wang, XPS and AES studies of the Cr/Al_2O_3 interface, Physica Status Solidi (a) 159 (1997) 425–437.